Paper No.
05625

CORROSION 2005

CO_2 / H_2S CORROSION UNDER SCALE FORMING CONDITIONS

Bruce Brown, Srdjan Nesic
Institute for Corrosion and Multiphase Technology
Ohio University
Athens, Ohio 45701

ABSTRACT

Three different mild steel coupons with two different surface areas were exposed to a CO_2 saturated multiphase environment with a trace amount of hydrogen sulfide under supersaturated scale forming conditions designed to increase the probability of localized corrosion. Corrosion testing was conducted in the region of low supersaturation values for iron carbonate ($SS_{FeCO3} < 10$) and three different supersaturation values for iron sulfide ($2.5 < SS_{FeS} < 125$) through adjustment of the partial pressure of H_2S during 30 day exposures to system conditions. Experiments were conducted in a 1% NaCl solution at 60ºC, pH 6.0, 0.77MPa partial pressure CO_2 with trace amounts of H_2S in both single phase flow (V_{sl} = 1 m/s) and multiphase flow (V_{sg}=3 m/s, V_{sl}= 1 m/s). Under the conditions tested, both siderite and mackinawite films were developed as adherent corrosion product films. Localized corrosion was observed.

Keywords: hydrogen sulfide, carbon dioxide, acid gas, multiphase flow, single-phase flow, supersaturation, localized corrosion, iron sulfide, iron carbonate.

INTRODUCTION

The previous series of experiments[1] was conducted to determine the effect of an incremental change in the solution pH (from 4 to 6.6) on CO_2 corrosion rates of UNS C1018 steel in the presence of H_2S in both single phase flow (V_{sl} = 1 m/s) and multiphase flow (V_{sg}=3 m/s, V_{sl}= 1 m/s) in a large scale multiphase flow loop. Protective adherent films, seen over the entire range of pH, limited corrosion rates in both single phase and multiphase flow conditions, but localized corrosion was not observed.

Experimentation in horizontal wet gas flow by Sun[2] has shown a relationship between partially protective iron carbonate films and an increase in localized corrosion near the saturation point for iron carbonate in solution. Therefore, this absence of localized corrosion in the previous series of experiments[1] raised questions about whether test exposure time or the addition of hydrogen sulfide affected the possibility of localized corrosion.

To increase the probability of observing localized corrosion in the experiments, changing exposure time and surface area was explored. Localized corrosion was observed within 30 days for experiments near the saturation point for iron carbonate in solution[2] so the experimental exposure time set at 30 days with coupons removed at 10 day intervals. And a 7.2 cm^2 surface area coupon was added to the experimental procedure to address the concerns that the 1.0 cm^2 coupon surface previously used was a significant factor in developing localized corrosion.

In this series of experiments, the calculated supersaturation value for iron carbonate was maintained near the saturation point (SS_{FeCO3} = 1) while the calculated supersaturation value of iron sulfide is altered. Corrosion rates from linear polarization resistance measurements and weight loss coupon analysis are compared, along with surface analysis of the coupons, to observe the type of films developed. An additional focus of this study is a better understanding of the iron sulfide / iron carbonate mixture films that occur due to precipitation of both species.

EXPERIMENTAL PROCEDURE

Tests were conducted in a 1% NaCl solution at 60ºC, 0.77MPa CO_2 partial pressure, with superficial liquid and superficial gas velocities set at 1m/s and 3m/s, respectively, in a closed system (Table 1). A 1950-liter volume, 0.10 m I.D., multiphase flow loop, the "Hydrogen Sulfide System," was used to provide a very stable environment for reproducible flow rates in single phase and multiphase flows.

The procedure for operation and experimentation of the Hydrogen Sulfide System is outlined in a previous study.[3] All experimental parameters, such as pH, temperature, partial pressures, and iron concentration, are adjusted and/or measured for stable conditions prior to the insertion of all flush mounted probes.

Seven probes were inserted in three test sections for exposure to single phase and multiphase flow regimes under identical fluid conditions. Two, flush-mounted, three-electrode probes in a concentric ring arrangement were used for linear polarization resistance (LPR) measurements, one in each flow regime. Two flush-mounted arrangements of four 0.457" diameter mild steel coupons press-fit into nylon holders were used for the "small" weight loss (WL) coupons in each flow regime. In this arrangement, three of the small WL coupons are UNS C1018 and one is X65 for each nylon holder. The last three ports (one per test section) each hold a single, 1.25" diameter, X65(2) coupon coated with non-conductive paint on all surfaces except for the flush mounted surface. All coupons were polished to a 600 grit finish, cleaned, dried, and weighed before insertion. LPR, "small" WL and one X65(2) coupon remained in the system for the entire 30 day exposure, while two of the 1.25" diameter X65(2) coupons are replaced with new coupons after the first 10 days of exposure: one in single phase, one in multiphase. All probes are flush mounted in the 6 o'clock position.

The WL material's chemical composition is given in Table 2. The 0.457" diameter coupons have a 1.06 cm^2 exposed surface area; while the 1.25" diameter coupons have a 7.24 cm^2 exposed surface area. Clarke solution cleaning[4] of the WL coupons was used for the weight loss procedures. General corrosion values were calculated by subtracting the initial coupon weight from the final coupon weight after Clarke solution cleaning of films. Localized corrosion rate values were determined by cross-section analysis and calibrated metallurgical microscope depth measurements.

LPR measurements were taken using an electrochemical measurement system and concentric ring probes with a UNS C1018 working electrode. Data were collected for 30 days with the aid of a multiplexer switching from the single phase probe to the multiphase probe. The time for each probe measurement sequence was 4 hours, so each probe was tested 2 to 3 times per 24 hour period for the entire 30 day testing period.

Iron concentration was determined by using a calibrated spectrophotometer. Since the Hydrogen Sulfide System does not have a means to control dissolved iron concentration, this parameter was measured "as is." Ten milliliters of sampled solution taken from the system was mixed with iron phen-anthroline reagent to produce a change in color directly related to the concentration of iron in solution.

H_2S concentration in the gas phase was measured with a piston pump and low range sensitive colormetric tubes. A needle valve was used to release gas from the gas phase of the large scale system into a directional tube where the measurement took place before the gas was vented. The length of color change in the detection tube reagent was measured using calipers to increase the accuracy of the value. Repeatability of this method was found to be ±5%.

During these experiments, carbon dioxide was the dominant gas, and, therefore, was an easily maintained parameter so that the carbonate concentration was somewhat constant. The H_2S concentration was reduced by purging with CO_2 at a constant system total pressure or increased by addition of pure H_2S at less than 10cc/min through a mass flow meter.

The three major factors that determine the magnitude of supersaturation for iron carbonate and iron sulfide are the ferrous ion concentration, $[Fe^{++}]$ which is the common ion, the carbonate ion concentration, $[CO_3^{-}]$, and the sulfide ion concentration, $[S^{2-}]$. The ferrous ion concentration is a measured value, while the carbonate ion and sulfide ion concentrations are calculated using thermodynamic relations and based on the partial pressures of CO_2 and H_2S in the gas phase, respectively.

Calculations

Bulk saturation values for iron sulfide, SS(FeS), were calculated using the solubility product,

$$pKsp(FeS) = 2848.779/T - 6.347 \qquad (1)$$

with temperature (T) in Kelvin, by Benning, et al.,[5] and concentrations based on the physicochemical model of CO_2 corrosion of mild steel.[7] The iron sulfide saturation value was calculated as:

$$SS(FeS) = \frac{[Fe^{2+}][HS^-]}{[H^+]Ksp(FeS)} \quad (2)$$

The bulk saturation value for iron carbonate, $SS(FeCO_3)$, was calculated using the equation for solubility product, [6]

$$Ksp(FeCO_3) = -\frac{10.13 + 0.0182 \cdot T}{0.0115 \cdot I^{-0.6063}} \quad (3)$$

with temperature (T) in ºC and ionic strength (I) in mol/L.

Using species concentrations based on the physicochemical model of CO_2 corrosion of mild steel,[7] the saturation value for iron carbonate was calculated as:

$$SS(FeCO_3) = \frac{[Fe^{2+}][CO_3^{2-}]}{Ksp(FeCO_3)} \quad (4)$$

Since saturation values measured during this experiment were always greater than one (1), the system was always "supersaturated" to some degree and values will be designated as "SS."

RESULTS

Since calculated values of supersaturation given in this report are dependent upon measured concentrations of iron and partial pressures, the change of values for these parameters over time are shown in Figure 1 for the first experiment, in Figure 14 for the second experiment, and in Figure 21 for the third experiment.

In these experiments, calculated and measured corrosion rates varied by an order of magnitude within the same experimental conditions; therefore, all corrosion rate data are displayed on a log scale.

Experiment 1

Based on the H_2S and Fe^{2+} concentrations measured (Figure 1), in Figure 2 the supersaturation values for Experiment 1 as calculated by Equations 2 and 4 is shown. From these calculations, the average value for iron sulfide supersaturation SS(FeS) = 7 was almost equivalent to the value for iron carbonate supersaturation $SS(FeCO_3)$ = 9 during Experiment 1; therefore, it was expected that the surface films

should contain a mixture of both precipitates. The partial pressure of H_2S varied slightly between 0.1 Pa and 0.2 Pa and the iron concentration diminished during this experiment, from 10 ppm ± 2 ppm in the beginning to 4 ppm ± 0.2 ppm by the end of 30 days.

Corrosion Rate Data. Figure 3 shows a plot of corrosion rate with time as measured by LPR to observe trends in the change in corrosion rate due to exposure time. The larger symbols on the graph represent the large-surface-area X65(2) coupons and are located at the exposure time of removal (x-coordinate) and the corrosion rate determined (y-coordinate). The first fact that can be observed from Figure 3 is that the trace amount of H_2S (<20ppm) in the system at pH 6 has produced an immediate reduction in the corrosion rate as compared with a "pure" CO_2 system. After the LPR probes were inserted, the amount of time necessary to obtain a stable open circuit potential (~30 min) was enough time for the solid state reaction (formation of a Mackinawite film) to retard corrosion in both single phase and multiphase flow regimes. The initial corrosion rates were 0.16 mm/yr for the single phase probe and 0.12 mm/yr for multiphase probe which reached a maximum of 0.23 mm/yr and 0.25 mm/yr, respectively, within two hours of exposure time. "Pure" CO_2 corrosion rates measured by LPR under conditions of 0.79 MPa CO_2, 60°C, pH 4, in synthetic seawater have been reported[8] with an initial value of 15 mm/yr with a stable corrosion rate of 8 mm/yr.

From Figure 3, it can also be seen that a good correlation exists between the weight loss values for the C1018 coupons and LPR measured for single phase flow. The error bars for the C1018 weight loss coupons represent the maximum and minimum corrosion rate and the data point is the average for each set of coupons. Integration of the LPR values for Experiment 1 gives 0.076 mm/yr in single phase and 0.018 mm/yr in multiphase as compared to 0.072 mm/yr in single phase and 0.058 mm/yr in multiphase for C1018 weight loss coupons. Comparison of weight loss corrosion rate results in Figure 4 shows that localized corrosion was only observed for the larger coupons.

It is inferred from the corrosion rate measurements in Experiment 1 that the material of construction and/or the exposed surface area played a part in the relationship between the LPR measurements and the small coupon weight loss measurements. It can also be inferred that a very adherent film formed on the surface of the LPR probe in the multiphase flow and affected the electrochemical measurements because these values were not reflected by the WL coupons in the same location.

Surface Analysis. The film formed on the surface of the coupons under these conditions proved to be weak and non-protective. The X65(2) WL coupon from multiphase flow, as shown in Figure 5, was removed after 10 days of exposure to system conditions and shows signs of flow induced degradation of the film. The same type of coupon exposed for 20 days also shows an increase in the amount of damage that occurred to the film (Figure 6). While inspecting the X65(2) coupon that was exposed for 20 days (Figure 6), a comparison of the damage on the film surface to the damage of the underlying base material of the same coupon shows that flow induced localized corrosion (FILC) did occur.

Measured film depth for cross sections of the X65(2) coupon exposed for 30 days show a large film deposition and localized corrosion. Figure 7 shows film deposition of approximately 100μm in the cross-section and Figure 8 shows localized corrosion for the same coupon under an uneven film surface that ranges from 60μm in depth to 120μm in depth.

Figure 9 provides a comparison between an SEM image and a backscatter SEM image for the same location on the X65(2) coupon exposed for 30 days. The corrosion product layer does not have an

easily discernable crystal structure, but does seem to have porosity as shown by color changes in the backscatter SEM. Both the SEM image and the backscatter SEM image show active pit growth in three locations after this exposure time. The dark locations in the pit areas of the backscatter SEM are proof of an existing detached film area where corrosion is occurring.

In contrast to the corrosion rates and film thickness measured on the X65(2) coupons, the smaller coupons had a lower corrosion rate and a correspondingly thinner corrosion product layer as shown in Figure 10. The immediate urge would be to suggest that the surface area of the material is a major factor because X65 was used for both large and small weight loss coupons. However, examination of the material composition in Table 2 shows a greater compositional similarity between X65 and C1018 (14 of 22) than between X65 and X65(2) (12 of 22). Chromium, molybdenum, and nickel are considered to be important for corrosion resistance, but are more abundant in the larger sample where the higher instance of localized corrosion occurred. Refer back to Figure 4 as a comparison of each material's corrosion rate to support the fact that the small X65 and the C1018 weight loss coupons had similar corrosion rates under similar conditions.

Film Analysis. The next important piece of information would involve the composition of the corrosion product film. Electronic Dispersion Spectroscopy (EDS) detected sulfur and iron elements in the film as expected. X-Ray Diffraction (XRD) was used and measurable peaks indicated a crystal structure present in the films. Analysis is done by comparison to standard XRD spectra and is represented by the peaks of intensity vs. Bragg angle (2θ). Comparison shows four matches for pyrrhotite at $2\theta = 31.5°$, 44.0°, 52.1°, and 65.0° (Figure 11) and five of eight major peaks correlated for siderite (Figure 12) at $2\theta = 24.9°$, 32.1°, 42.4°, 52.9°, and 61.8°.

The conclusion from XRD results is that pyrrhotite films and iron carbonate (siderite) films were formed on the coupon surface under the recorded conditions as seen in Figure 13.

Experiment 2

Using the decrease in iron concentration during the first experiment, and by maintaining lower hydrogen sulfide partial pressures from 0.05 Pa to 0.15 Pa as shown in Figure 14, the saturation values for iron sulfide were kept below that of iron carbonate during the second experiment as calculated in Figure 15. The integrated average values of supersaturation are 3 for iron sulfide and 6 for iron carbonate. Therefore, surface films should be more influenced by iron carbonate precipitation than by iron sulfide precipitation. During this experiment, the iron concentration increased 2.0 ppm from 3.5 ppm ± 0.2 ppm at start-up to 5.5 ppm ± 0.2 ppm at the end of 30 days.

Corrosion Rate Data. Note the small variance in corrosion rates as seen by LPR and WL in Figure 16 and illustrated by the bar graph weight loss values in Figure 17 (Note: Corrosion rate data are on a log scale.). Again, the realization that a trace amount of H_2S in the system, (< 0.2 Pa) at pH 6 has produced an immediate reduction in the corrosion rate by solid state reaction (formation of a Mackinawite film) which retards corrosion. Integration of the LPR values for Experiment 2 gives 0.012 mm/yr in single phase and 0.243 mm/yr in multiphase as compared to 0.037 mm/yr in single phase and 0.397 mm/yr in multiphase for C1018 weight loss coupons. The initial LPR corrosion rates were 0.048 mm/yr for the single phase probe and 0.097 mm/yr for the multiphase probe. In this case,

the single phase corrosion rate dropped and remained almost constant at 0.01 mm/yr while the multiphase had similar increase and decrease in the LPR measurements within the first hour of exposure to the system. The multiphase LPR measurements increased from 0.097 mm/yr to 0.17 mm/yr within the first hour of exposure with a slight drop in corrosion rate to 0.145 mm/yr after 1 hour.

Surface Analysis. The lack of film formation on the surface of the coupons, due to the lower bulk saturation values for both iron carbonate and iron sulfide, coupled with a very low corrosion rate, minimized the damage to the surface of the coupons and the possibility of localized corrosion.

In comparison to Figure 7 and Figure 8, the film formed throughout the second experiment was only 30μm, or 30% to 50% of the film formed during the first experiment. The cross sections of the film measured after the 30 day exposure for Experiment 2 are shown in Figure 18 for the larger surface area X65(2) coupon and in Figure 19 for the smaller C1018 weight loss coupon.

Film Analysis. Figure 20 shows the comparison to previous film analysis for XRD peak determinations. The graph shows a similar comparison of films formed in single phase and multiphase to pyrrhotite and siderite peak XRD locations. So even though a minimal film formed under these test conditions, it consisted of similar crystal structures.

Experiment 3

During experiment 3, the iron concentration varied from 20 ppm at the beginning of the experiment to 15 ppm at the end of 25 days and the hydrogen sulfide concentration in the gas phase averaged 1340 Pa over the length of the experiment with lows around 1250 Pa and high values to 1500 Pa, shown in Figure 21. Calculated saturation values of $SS(FeCO_3)$ and SS(FeS) for the length of the experiment are shown in Figure 22. The SS(FeS) averaged 17.2 times greater than the $SS(FeCO_3)$, so a log scale is used for visualization.

Corrosion Rate Data. As seen in Figure 23, corrosion rates measured by LPR for multiphase (MP) were less than 1 mm/yr as expected, but the single phase (SP) LPR measurements dramatically increased with the first few days of testing. This was assumed to be caused by conductive FeS films and not actual measured corrosion rates. The film growth produced highly conductive film between the working and counter electrodes of the LPR probe within the first five (5) days of experimentation. This conductive film acted as an electrical short with a very low resistance which affected the value of the measured solution resistance. This would also account for the extremely low polarization resistance (Rp) measured, which would provide false information leading to the extremely high calculated corrosion rates as seen in Figure 23. The probes were not disturbed in order to monitor the film's resistance to consistent system flow conditions with time and the WL coupon that would experience the same conditions would be removed after the first 10 days exposure for verification.

A cross-sectional view of a small WL coupon exposed to multiphase flow is shown in Figure 24. The base film is a uniform 20μm film with an additional layer of broken fragments on top. As shown in the surface SEM of Figure 25, the secondary film has broken areas which have been assumed to lead to

localized corrosion should they be removed by flow. The light colored top film is fragmented here due to drying after removal from system conditions.

Corrosion rates were lower overall in single phase flow as compared to multiphase flow in the Experiment 3 as measured by weight loss; see Table 3. There was no localized corrosion observed in Experiment 3. As seen in Figure 26, the small diameter coupons had corrosion rates based on weight loss equivalent to 0.20 ± 0.01 mm/yr for two C1018 coupons in single phase flow and 0.59 ± 0.01 mm/yr for two C1018 coupons in multiphase flow. X65 small diameter coupons also provided similar corrosion rate results with 0.33 mm/yr in single phase flow and 0.56 mm/yr for multiphase flow.

The larger 7.24cm^2 surface area coupons seemed to have overall higher corrosion rates than did the small coupons, but this could be due to the shorter length of exposure to system conditions. If the corrosion attack only happens within the first few hours of exposure to system conditions, then by extending the amount of time, the corrosion rate decreases with time. This is seen in Figure 27 for coupons exposed to single phase conditions and in Figure 28 for coupons exposed to multiphase conditions.

Surface Analysis. Film developed under single phase conditions on the small coupons would seem to be thicker and more dense (Figure 29), as compared to the film developed in multiphase conditions, Figure 24. The surface of the single phase WL coupon film, Figure 30, also appears to feature a more uniform coverage of the surface as compared to the surface of the multiphase WL coupon film, Figure 25. Both aspects, "uniformity" and "coverage," would aid in the conductivity of the film showing similarities between the WL coupon film and that measured on the LPR in single phase flow.

Film Analysis. XRD provided a similar comparison of films formed in single phase and multiphase to pyrrhotite and siderite peak locations, but electron dispersion spectroscopy (EDS) provided new information on the thicker film. EDS spot analysis of a film developed after the 25 day exposure to system conditions in multiphase flow shows that sulfides in the film reside mainly in the upper layers near the solid/fluid interface.

A cross-sectional view of the coupon in Figure 31 shows three layers of film developed on the surface. From the surface of the coupon outward, the first 60 micron layer was analyzed with EDS and found to have 0% Sulfur, 40% Iron, 13% Carbon, and 30% Oxygen. The next 60 micron layer was found to have 0% Sulfur, 45% Iron, 13% Carbon, and 16% Oxygen. The outermost 30 micron layer was found to have 11% Sulfur, 33% Iron, 22% Carbon, and 13% Oxygen. These values are also shown in Table 4. It can be concluded from these results that the mechanisms of film growth under the conditions tested produce an iron carbonate film near the metal surface while the iron sulfide film resides in the surface layer near the bulk solution. Modeling of these mechanisms is currently under investigation.

Comparison of Experimental Results

WL coupons. Visual inspection of corrosion coupons removed at intervals of 10, 20, and 30 days, reinforce the difference in the supersaturation values of each experiment. Figure 32 shows the surface of the coupons, as removed from the system after exposure, for the first experiment. Figure 33 shows the surface of the coupons, as removed from the system after exposure, for the second experiment.

Figure 34 shows the surface of the coupons, as removed from the system after exposure, for the third experiment. For the first and second experiment, the effect of flow on the corrosion product films can be seen on the surface of the coupon.

In Experiment 1, damage to the film was later shown to provide indications of localized corrosion in the base material. The film in this case has undergone damage with time and elongated features show the damage to be enhanced by flow on the corrosion product film. The kinetics for iron carbonate film formation were high enough in this experiment to precipitate a film on the surface which was competitive with the iron sulfide film formed. The non-homogeneous film would have areas of different porosities allowing localized corrosion.

With a lower iron carbonate supersaturation in Experiment 2, a film did not seem to form until the latter part of the experiment, but the corrosion rates experienced are still very low as compared to a system with no H_2S. The film could be a solid state film, such as mackinawite, that only requires a thin surface coverage to retard corrosion. The lack of corrosion product film during this experiment led to a general corrosion with no localized corrosion.

In Experiment 3, a very dark, dense film was formed within the first 10 days and maintained throughout the experiment. Visual observation from Figure 34 shows a darker colored film that produces less reflective light when photographed. This would seem to give an indication of a denser, closer packed surface film, but, this film was a non-protective film which had the highest general corrosion rates overall.

WL corrosion rates. Comparison of the corrosion rates for the large size, X65(2) WL coupons in Figure 35 shows localized corrosion in Experiment 1. Two trends can be seen in this graph. The first is that localized corrosion was increasing with time during experiment 1 and the second is that there is an increase general corrosion rate with an increase in hydrogen sulfide.

By observation of the corrosion rates for all of the smaller WL coupons (shown collectively in Figure 36), information collectively gained from the three experiments can be explained.

Although no localized corrosion was seen on the small coupons in Experiment 1, the mixture film produced limited the general corrosion rate and the effects of multiphase flow are not seen due to the buffering effect that the film has in the mass transfer of corroding species, that is to say, the corrosion rates in single phase and multiphase are very similar.

Experiment 2 had the lowest iron carbonate supersaturation value and shows the effect of mackinawite film on corrosion rate retardation in single phase flow by having the lowest overall corrosion rate in the three experiments. This same mackinawite film in experiment 2 does not limit the corrosion rate as well in the turbulence multiphase flow.

The highest corrosion rates were measured overall in Experiment 3. Since the iron sulfide supersaturation was 17.2 times greater than the iron carbonate supersaturation, the iron sulfide film would have been dominant. With an overall higher corrosion rate than the previous experiments, the film in Experiment 3 was more porous, but the corrosion rates between single phase and multiphase flow are very similar showing that a thick film exists, which limits mass transfer of corroding species.

CONCLUSIONS

1. Iron sulfide and iron carbonate supersaturation values are important parameters in defining the film morphology and predicting corrosion rates in systems containing hydrogen sulfide and carbon dioxide.

2. Corrosion rate retardation was observed due to mackinawite film formation under all experimental conditions containing small amounts of hydrogen sulfide.

3. Precipitated films, formed on top of existing mackinawite films, decreased the effect of flow, but increased the overall corrosion rate and the probability of localized corrosion.

4. Mechanisms of corrosion product film growth in film forming conditions containing carbon dioxide and hydrogen sulfide can produce multilayer films.

ACKNOWLEDGEMENTS

We would like to thank BP, ExxonMobil, Shell, TOTAL, ChevronTexaco, ConocoPhillips, ENI, Saudi Aramco, Champion Technologies, Clariant, MI Technologies, and Nalco, as Board members who have provided support for our research.

REFERENCES

1. Brown, B., Parakala, S.R., Nesic, S., "CO_2 Corrosion in the Presence of Trace Amounts of H_2S," NACE Corrosion 2004, paper no. 04736.

2. Sun, Y., "Localized Corrosion in Horizontal Wet Gas Flow," Ohio University, PhD dissertation, June 2003.

3. Brown, B., Schubert, A., "The Design and Development of a Large-Scale Multiphase Flow Loop for the Study of Corrosion in Sour Gas Environments," NACE Corrosion 2002, paper no. 02502.

4. ASTM G1-81, "Standard Practice for Preparing, Cleaning, and Evaluating Corrosion Test Specimens," Laboratory Corrosion Tests and Standards, Editors: Haynes, G.S., Baboian, R., pp505-509, section 7.7.2, 1985.

5. Benning, L.G., Wilkin, R.T., Barnes, H.L., "Reaction pathwasy in the Fe-S system below 100ºC," Chemical Geology, v. 167, 2000, pp25-51

6. IUPAC: Chemical Data Series No. 21, Stability constants of Metal-Ion Complexes. Par A: Inorganic ligands. Pergamon Press.

7. Nordsveen, M., Nesic, S., Nyborg, R., Stangeland, A., "A Mechanistic Model for Carbon Dioxide Corrosion of Mild Steel in the Presence of Protective Iron Carbonate Films – Part 1: Theory and Verification," Corrosion, May 2003, vol. 59, no. 5, pp 443 – 456.

8. Brown, B., Lee, K-L, Nesic, S., "Corrosion in Multiphase Flow Containing Small Amounts of H2S," NACE Corrosion 2003, paper no. 03341.

TABLES

Table 1. Experimental Test Matrix

Parameter	Conditions
CO_2 partial pressure	0.77MPa (7.7 bar)
Solution	1% NaCl solution, pH6
Corrosion Rate Measurement	Weight loss (C1018 and X-65) Linear Polarization Resistance
Single-phase flow Two-phase flow	V_{sl} = 1 m/s V_{sl} = 1 m/s, V_{sg} = 3 m/s
Temperature	60ºC
Test Time	30 days
H_2S concentration	Manually controlled, observed
Fe^{2+} concentration	As measured
Iron carbonate supersaturation	$1 < SS(FeCO_3) \leq 10$ (Exp 1) $1 < SS(FeCO_3) \leq 5$ (Exp 2) $1 < SS(FeCO_3) \leq 10$ (Exp 3)
Iron sulfide supersaturation	$1 < SS(FeS) \leq 10$ (Exp 1) $1 < SS(FeS) \leq 5$ (Exp 2) $100 < SS(FeS) \leq 150$ (Exp 3)

Table 2. Composition of weight loss materials used

Material Name	Al	As	B	C	Ca	Co	Cr	Cu
C1018	0.001%	0.007%	0.0005%	0.16%	0.007%	0.010%	0.063%	0.25%
X65	0.032%	0.005%	0.0003%	0.050%	0.004%	0.006%	0.042%	0.019%
X65(2)	0.032%	0.008%	0.001%	0.13%	0.002%	0.007%	0.14%	0.131%

Material Name	Mn	Mo	Nb	Ni	P	Pb	S	Sb
C1018	0.79%	0.02%	0.006%	0.078%	0.008%	0.016%	0.029%	0.011%
X65	1.32%	0.031%	0.046%	0.039%	0.013%	0.020%	0.002%	0.011%
X65(2)	1.16%	0.16%	0.017%	0.36%	0.009%	<0.001%	0.009%	0.009%

Material Name	Si	Sn	Ta	Ti	V	Zr
C1018	0.25%	0.017%	0.008%	<0.001%	0.001%	0.004%
X65	0.31%	0.001%	0.007%	0.002%	0.055%	0.003%
X65(2)	0.26%	0.007%	<0.001%	<0.001%	0.047%	<0.001%

Table 3. Weight Loss Corrosion Rates

Material [* - two coupons]	Location	Exposure time (days)	Surface area (cm^2)	Corrosion rate (mm/yr)
C1018 *	SP	25	1.06	0.20 ± 0.01
C1018 *	MP	25	1.06	0.59 ± 0.01
X-65	SP	25	1.06	0.33
X-65	MP	25	1.06	0.56
X-65(2)	SP	10	7.24	1.09
X-65(2)	MP	10	7.24	6.71
X-65(2)	SP	15	7.24	0.31
X-65(2)	MP	15	7.24	5.76

Table 4. Composition of surface film layers by EDS, 25 days, MP.

Element	Layer 1 (60um, next to surface)	Layer 2 (60 um, middle)	Layer 3 (30 um, next to solution)
Sulfur (S)	0	0	11
Iron (Fe)	40	45	33
Carbon (C)	13	13	22
Oxygen (O)	30	16	13
Trace elements	17	26	21

FIGURES

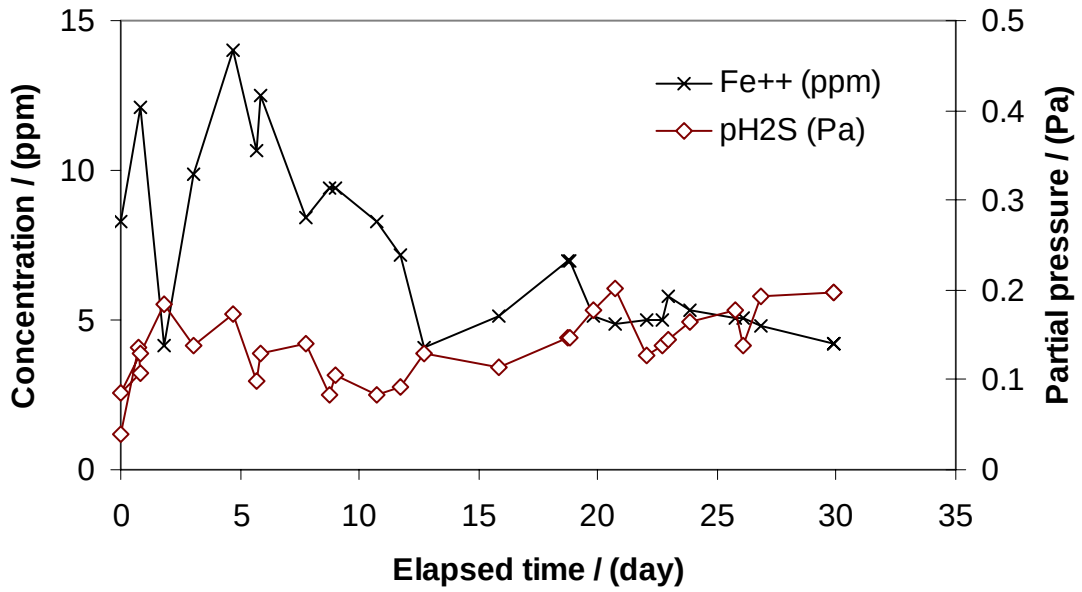

Figure 1. Experiment 1: Variations of iron and hydrogen sulfide concentrations with time. (60°C, 0.77 MPa CO_2, pH 6, H_2S gas phase concentration = 25 ± 10 ppm)

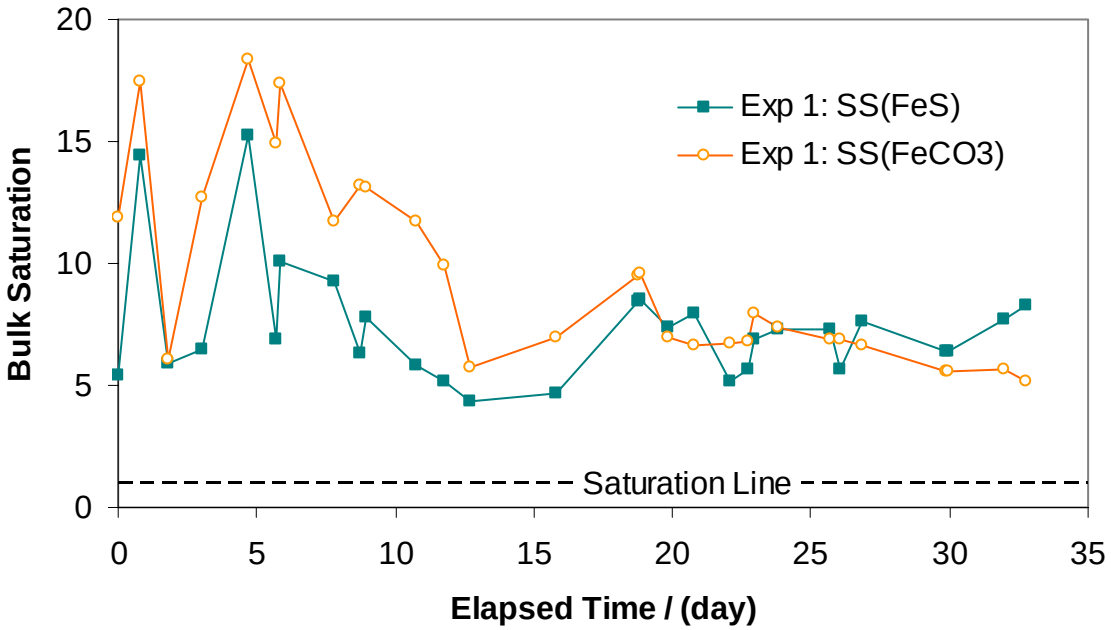

Figure 2. Experiment 1: Calculated values of supersaturation for iron sulfide and iron carbonate. (60°C, 0.77 MPa CO_2, pH 6, H_2S gas phase concentration = 25 ± 10 ppm)

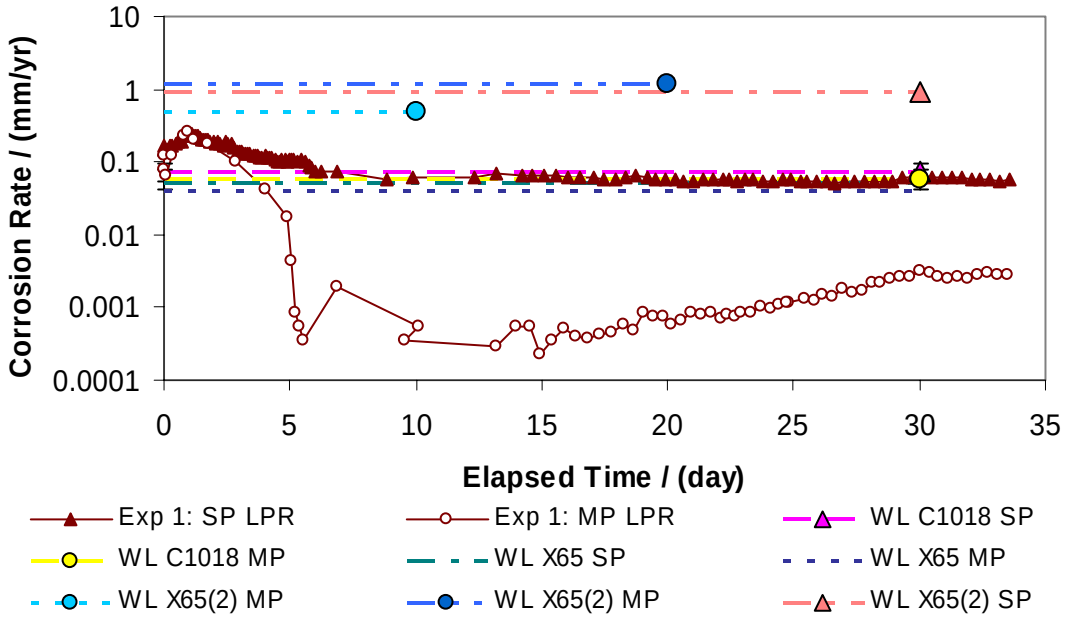

Figure 3. Experiment 1: Corrosion rate measurements by LPR and WL. (60°C, 0.77 MPa CO_2, pH 6, Vsg = 3m/s, Vsl = 1m/s, H_2S gas phase concentration = 25 ± 10 ppm)

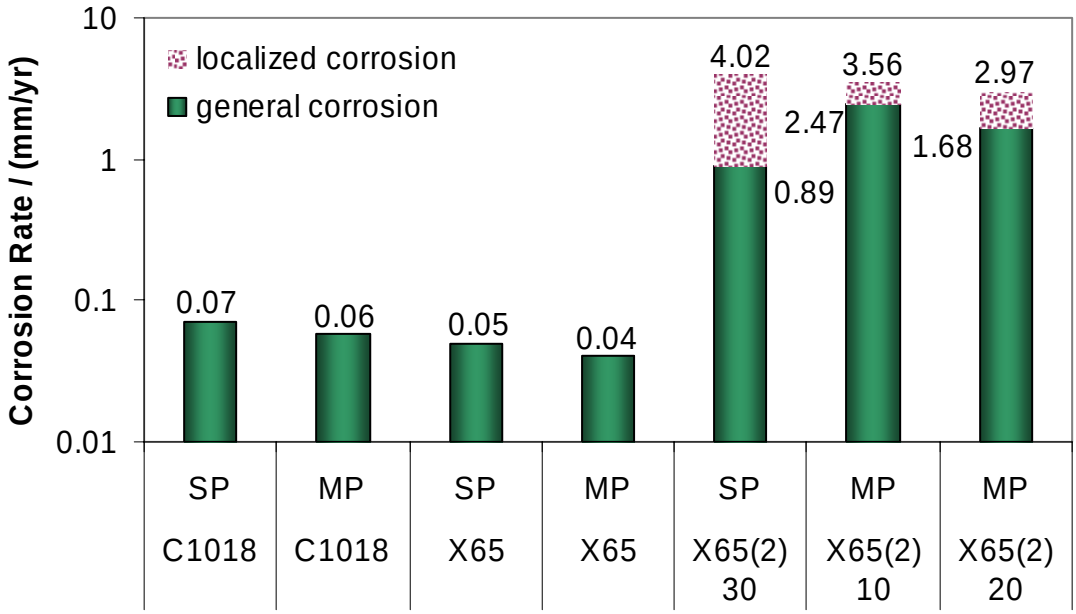

Figure 4. Experiment 1: Coupon weight loss comparison. (60°C, 0.77 MPa CO_2, pH 6, Vsg = 3m/s, Vsl = 1m/s, H_2S gas phase concentration = 25 ± 10 ppm, 10, 20, & 30 days)

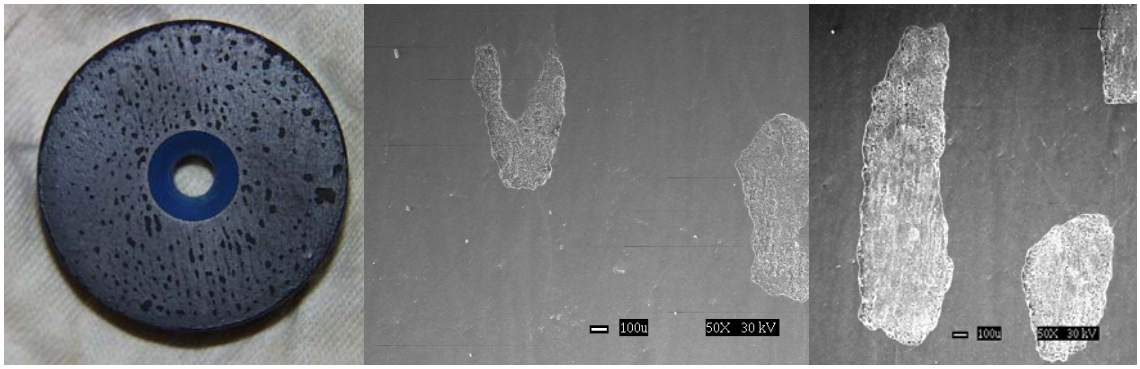

Figure 5. Experiment 1: X65(2), 10 day exposure to multiphase flow, examples of degradation of the film by fluid flow. Flow is in the "upward" direction of the picture. (60°C, 0.77 MPa CO_2, pH 6, Vsg = 3m/s, Vsl = 1m/s, H_2S gas phase concentration = 25 ± 10 ppm)

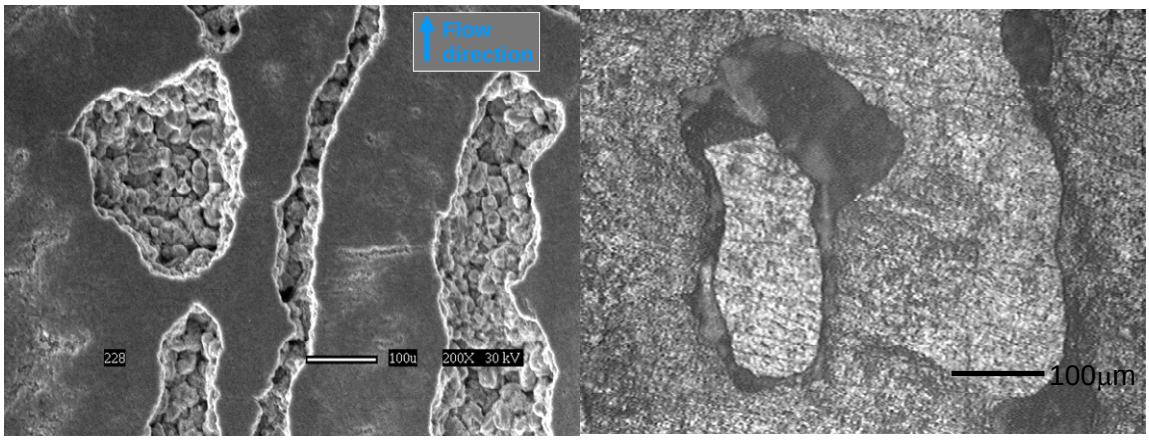

Figure 6. Experiment 1: X65(2) after 20 days exposure to multiphase conditions, examples of degradation of the film by fluid flow. Relationship shown between film disruption and substrate corrosion (FILC). (60°C, 0.77 MPa CO_2, pH 6, Vsg = 3m/s, Vsl = 1m/s, H_2S gas phase concentration = 25 ± 10 ppm)

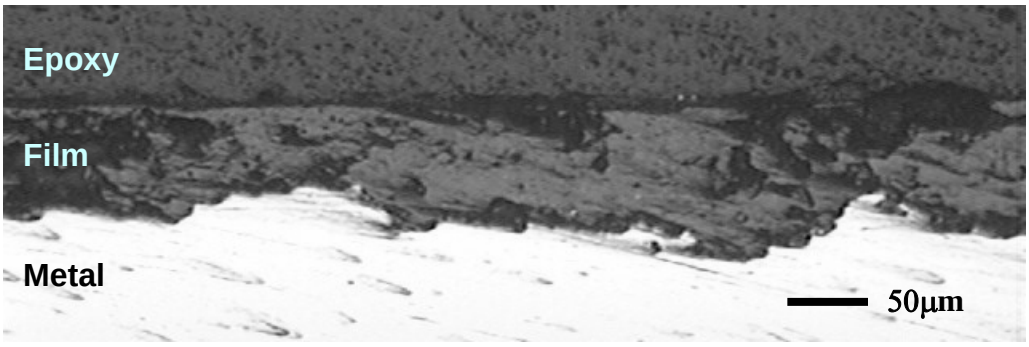

Figure 7. Experiment 1: X65(2), 30 day exposure to single phase flow, 52µm to 103 µm film thickness. (100X metallurgical microscope, 60°C, 0.77 MPa CO_2, pH 6, Vsg = 3m/s, Vsl = 1m/s, H_2S gas phase concentration = 25 ± 10 ppm)

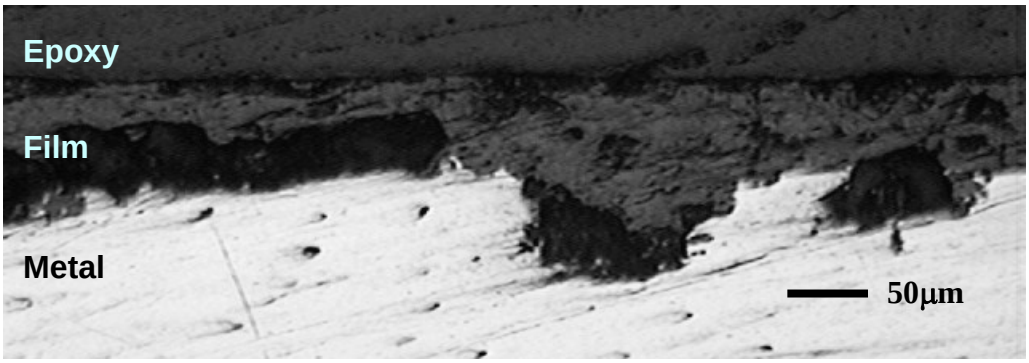

Figure 8. Experiment 1: X65(2), 30 day exposure to single phase flow, 60 to 125 µm film thickness, showing pitting. (100X metallurgical microscope, 60°C, 0.77 MPa CO_2, pH 6, Vsg = 3m/s, Vsl = 1m/s, H_2S gas phase concentration = 25 ± 10 ppm).

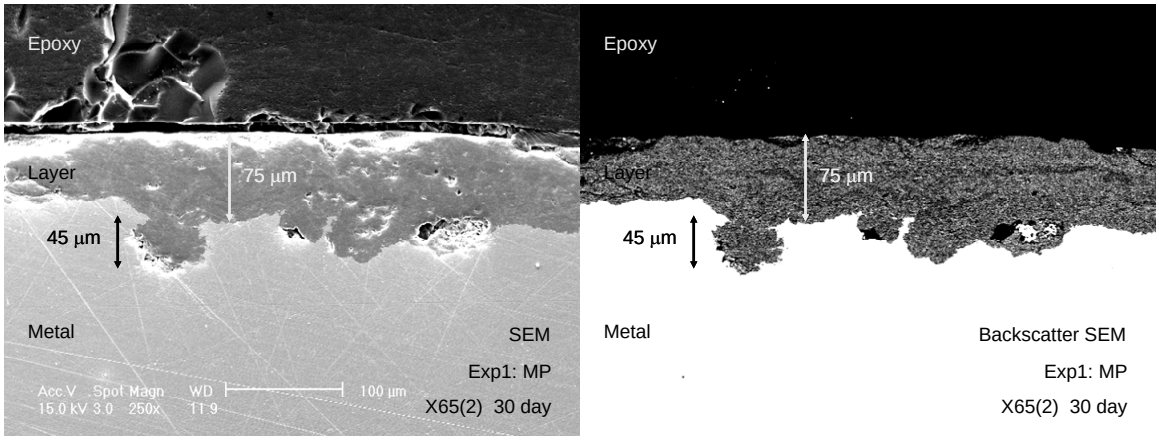

Figure 9. Experiment 1: Cross sectional analysis of X65(2) WL coupon from single phase flow, 30 day exposure, SEM and Backscatter SEM images showing pit growth under the film. (60°C, 0.77 MPa CO_2, pH 6, Vsg = 3m/s, Vsl = 1m/s, H_2S gas phase concentration = 25 ± 10 ppm)

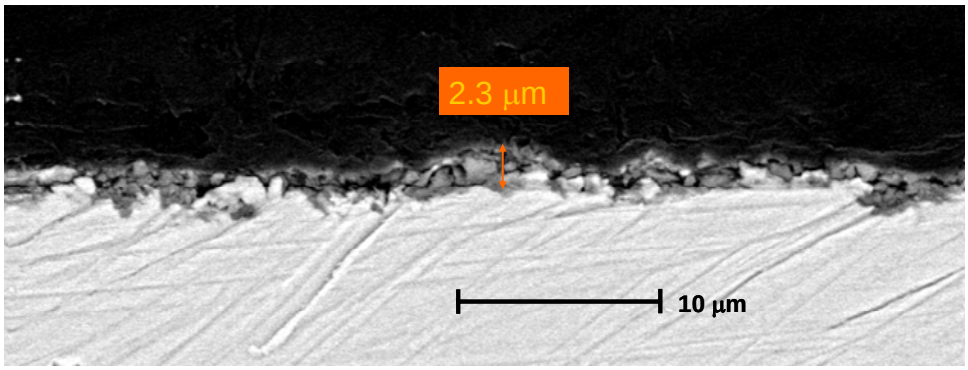

Figure 10. Experiment 1: C1018 weight loss coupon, 30 day exposure, backscatter SEM for definition of the corrosion layer. (60°C, 0.77 MPa CO_2, pH 6, Vsg = 3m/s, Vsl = 1m/s, H_2S gas phase concentration = 25 ± 10 ppm)

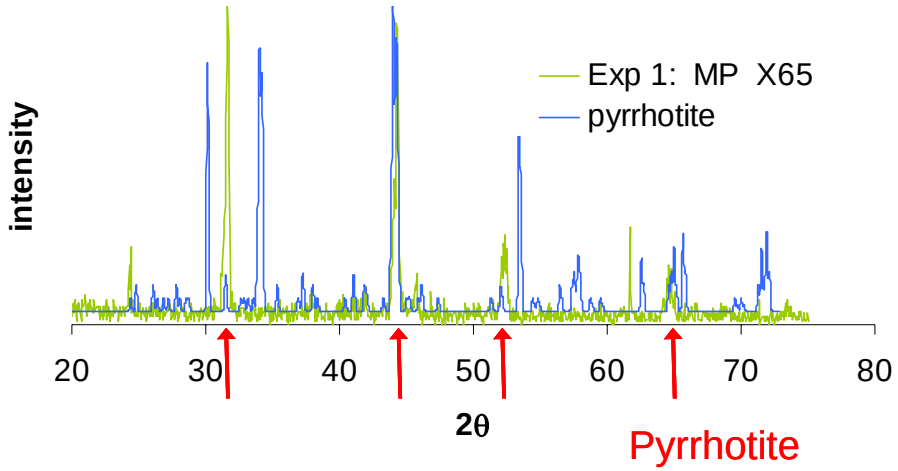

Figure 11. Experiment 1: XRD comparison with pyrrhotite reference. Peaks considered "matches" are designated with arrows. (60°C, 0.77 MPa CO_2, pH 6, H_2S gas phase concentration = 25 ± 10 ppm, 30 day exposure).

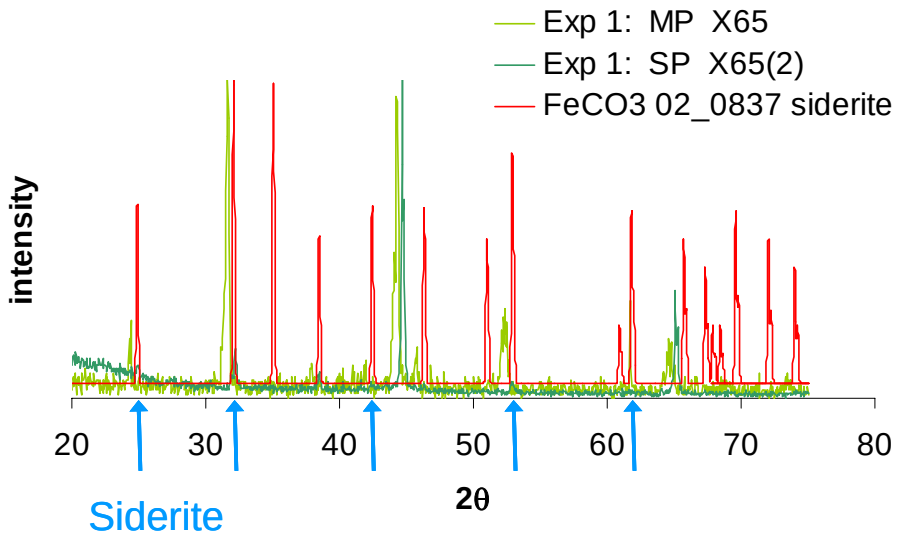

Figure 12. Experiment 1: XRD comparison with siderite reference. Peaks considered "matches" are marked with arrows. (60°C, 0.77 MPa CO_2, pH 6, H_2S gas phase concentration = 25 ± 10 ppm, 30 day exposure).

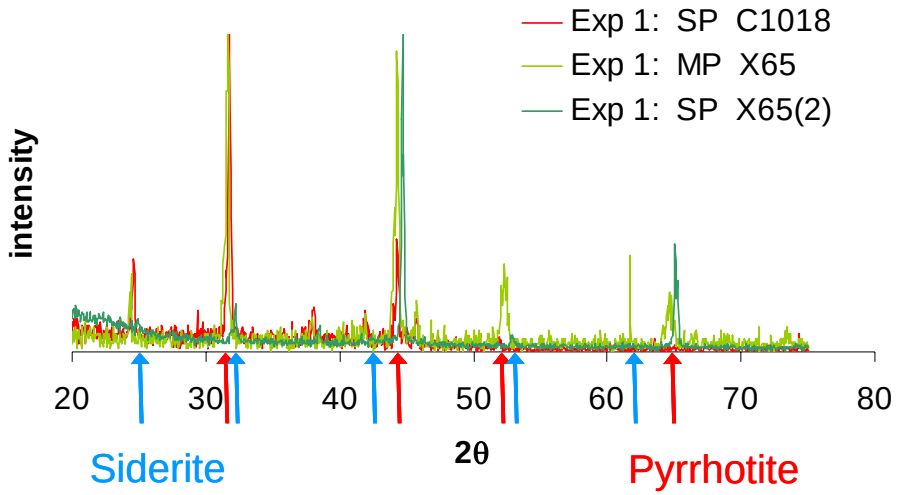

Figure 13. Experiment 1: XRD siderite / pyrrhotite mixture film. Peaks considered "matches" are marked with arrows. (60°C, 0.77 MPa CO_2, pH 6, H_2S gas phase concentration = 25 ± 10 ppm, 30 day exposure).

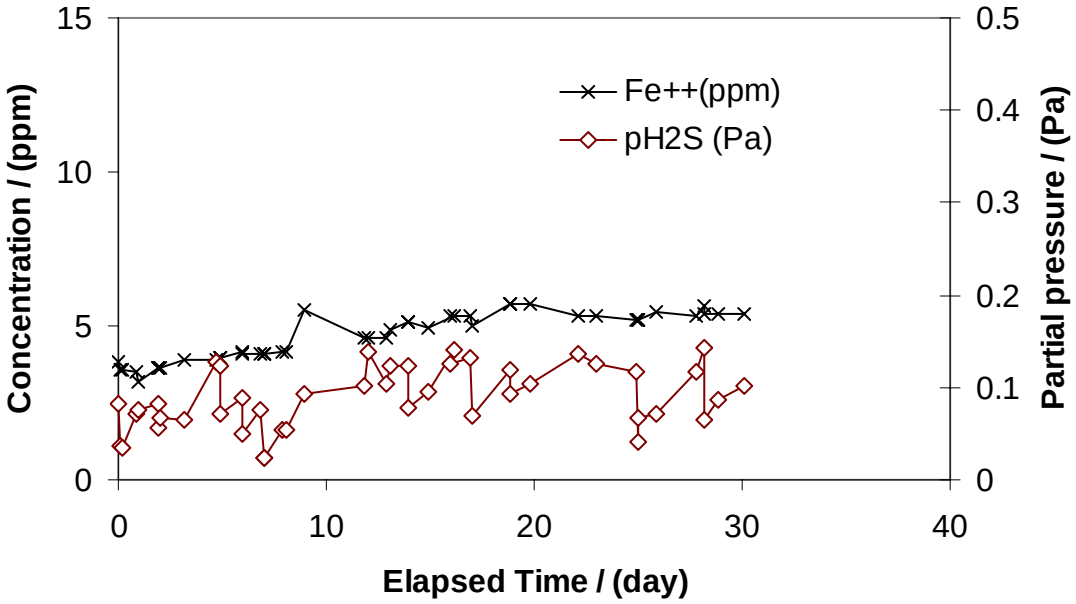

Figure 14. Experiment 2: Variations of iron and hydrogen sulfide concentrations with time. (60°C, 0.77 MPa CO_2, pH 6, 12 ± 5ppm H_2S).

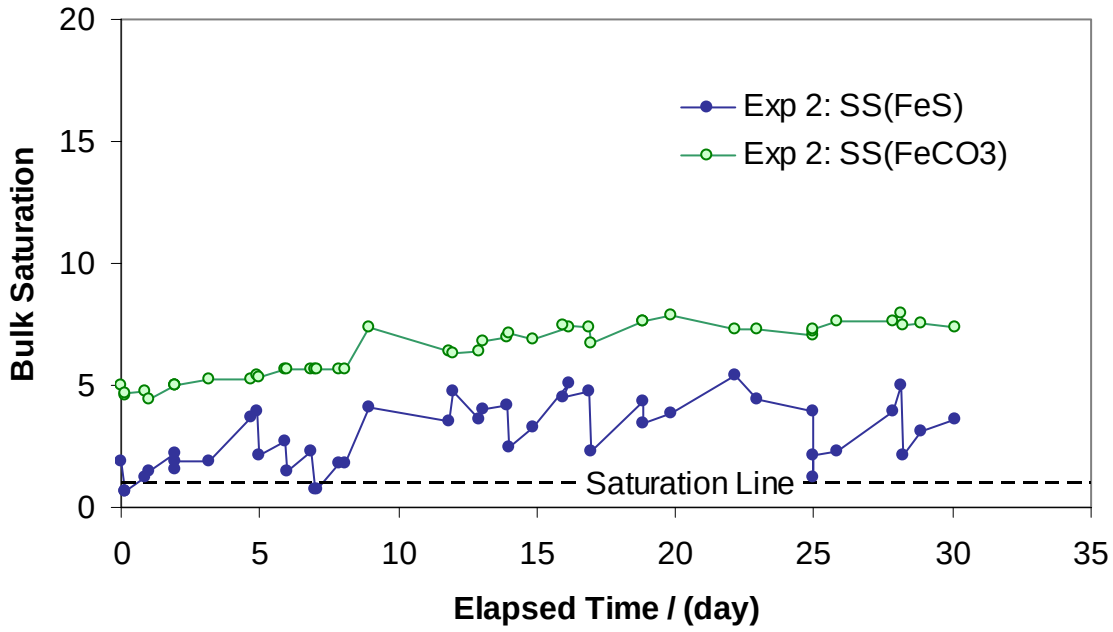

Figure 15. Experiment 2: Calculated values of supersaturation for iron sulfide and iron carbonate. (60°C, 0.77 MPa CO_2, pH 6, H_2S gas phase concentration = 12 ± 5 ppm)

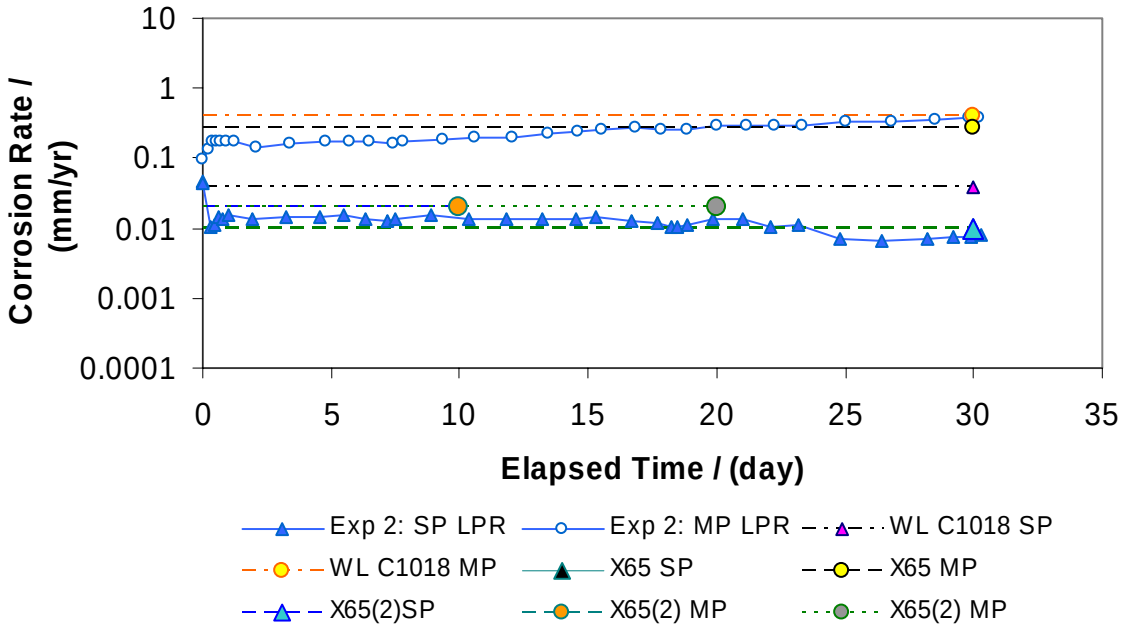

Figure 16. Experiment 2: Corrosion Rates measured by LPR and single C1018 WL values. (60°C, 0.77 MPa CO_2, pH 6, 12 ± 5ppm H_2S).

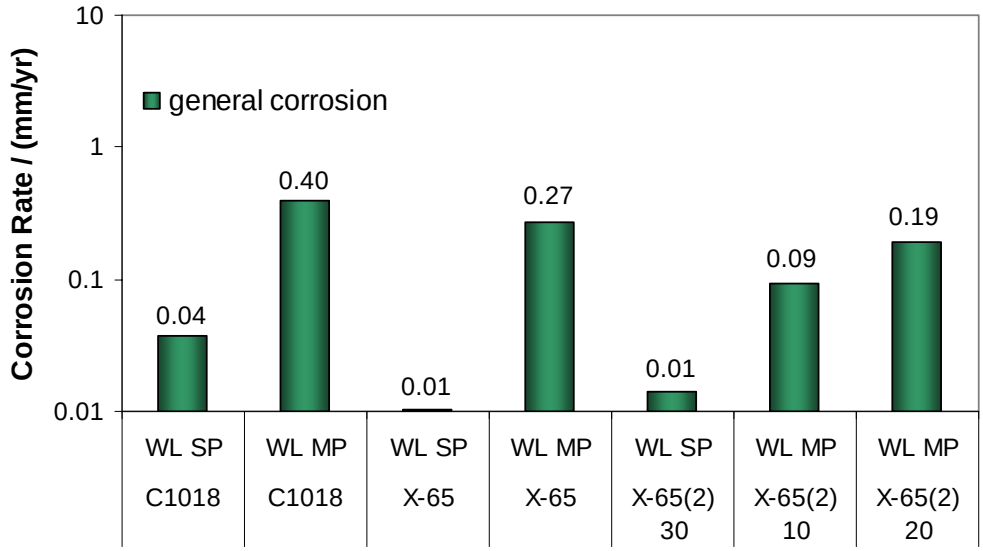

Figure 17. Experiment 2: Coupon weight loss comparison separated by material. (60°C, 0.77 MPa CO_2, pH 6, 12 ± 5ppm H_2S, 10, 20, and 30 day exposures).

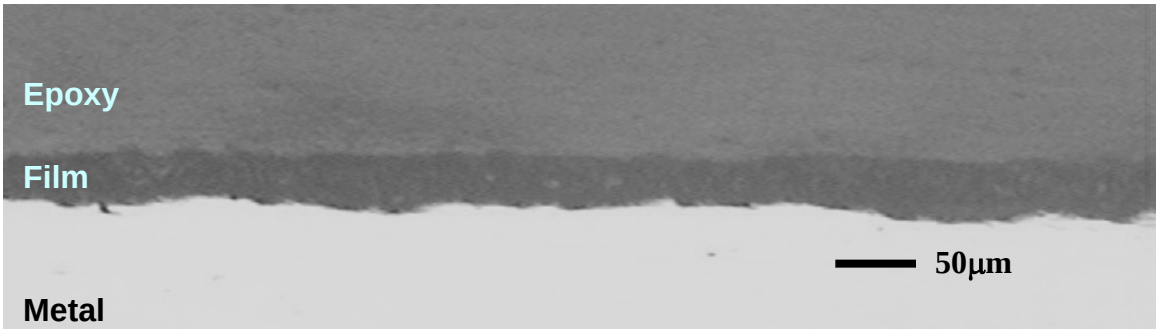

Figure 18. Experiment 2: Cross section of X65(2) WL coupon from multiphase flow exposure shows a 28 to 30 µm film thickness. (100X metallurgical microscope, 60°C, 0.77 MPa CO_2, pH 6, 12 ± 5ppm H_2S, 30 day exposure).

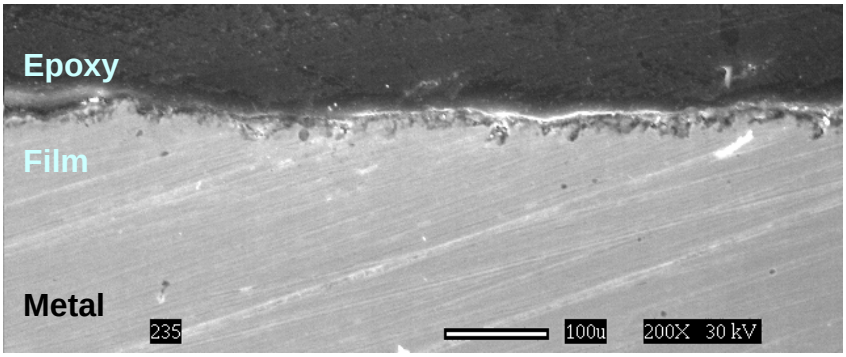

Figure 19. Experiment 2: Cross section of UNS C1018 WL coupon from multiphase flow exposure shows a 15 to 30 µm film thickness. (60°C, 0.77 MPa CO_2, pH 6, 12 ± 5ppm H_2S, 30 day exposure).

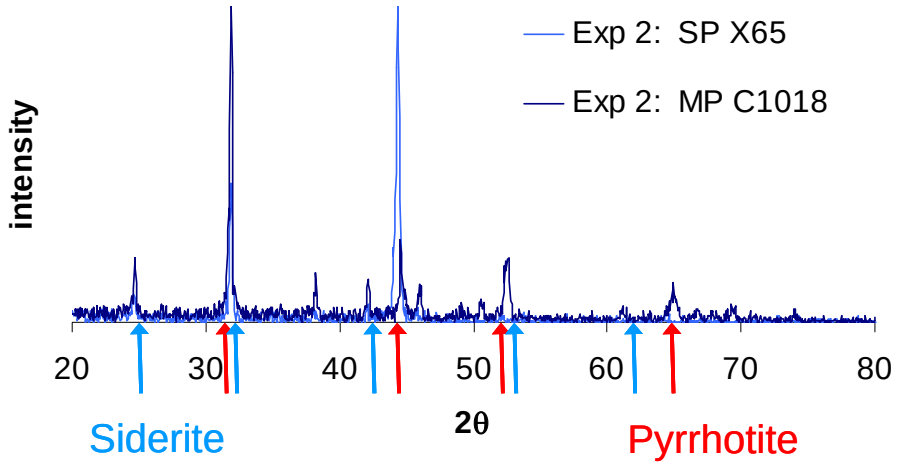

Figure 20. Experiment 2: XRD comparison from previous designation of siderite and pyrrhotite. Peaks considered "matches" are marked with arrows.

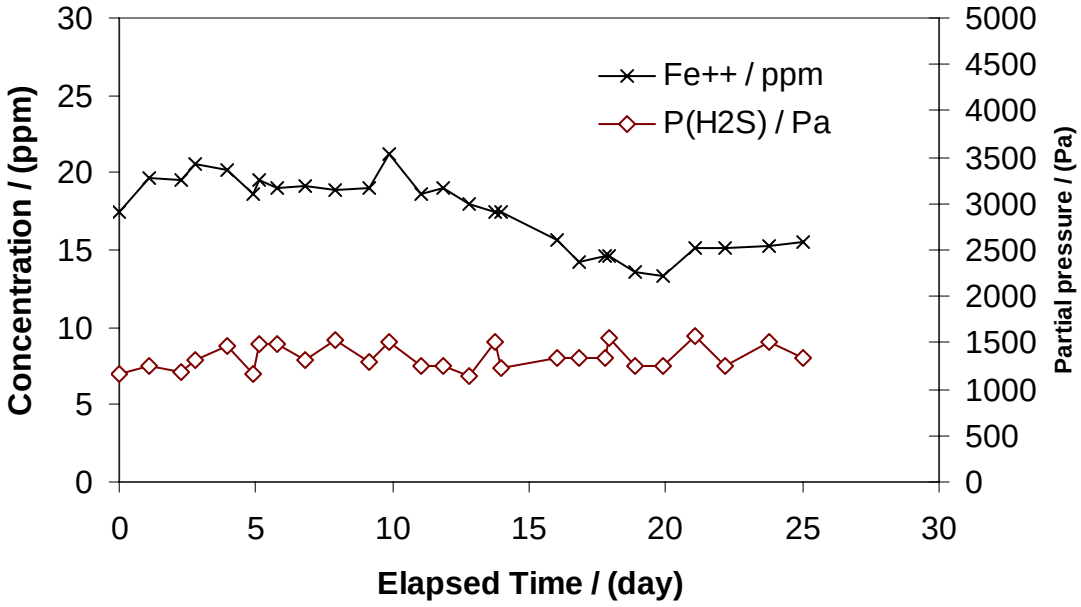

Figure 21. Experiment 3: Variations of iron and hydrogen sulfide concentrations with time. (60°C, 0.77 MPa CO_2, pH 6, 120 ± 10 ppm H_2S).

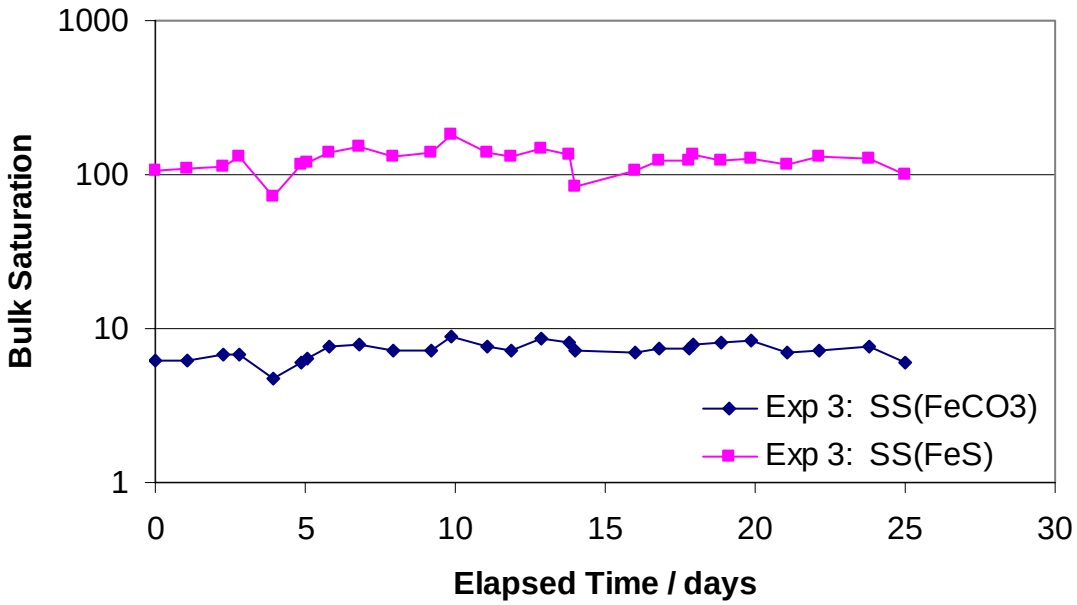

Figure 22. Experiment 3: Calculated values of supersaturation for iron sulfide and iron carbonate. (60°C, 0.77 MPa CO_2, pH 6, H_2S gas phase concentration = 120 ± 10 ppm)

.

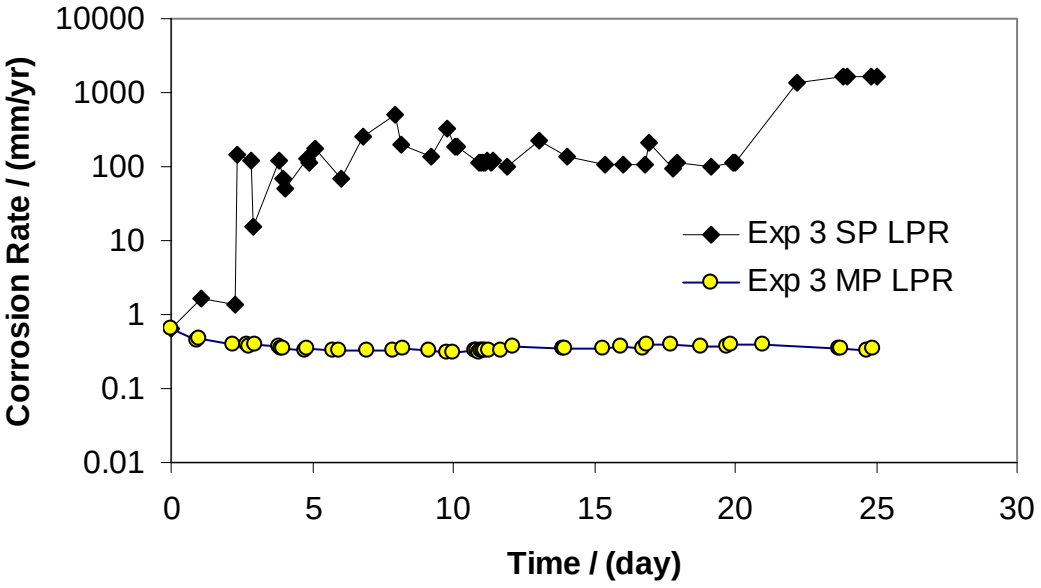

Figure 23. Experiment 3: Measured values for single phase LPR and multiphase LPR corrosion rate with time. Single phase LPR measurements affected by conductive FeS films (60°C, 0.77 MPa CO_2, pH 6, H_2S gas phase concentration = 120 ± 10 ppm)

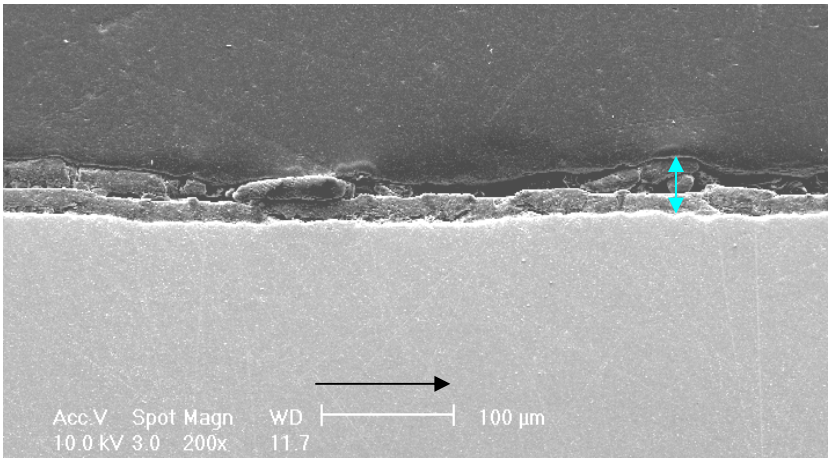

Figure 24. Experiment 3: Cross Section of small UNS C1018 WL coupon from multiphase flow. SEM at 200X magnification shows a 30µm total film thickness. (60°C, 0.77 MPa CO_2, pH 6, H_2S gas phase concentration = 120 ± 10 ppm, 25 day exposure).

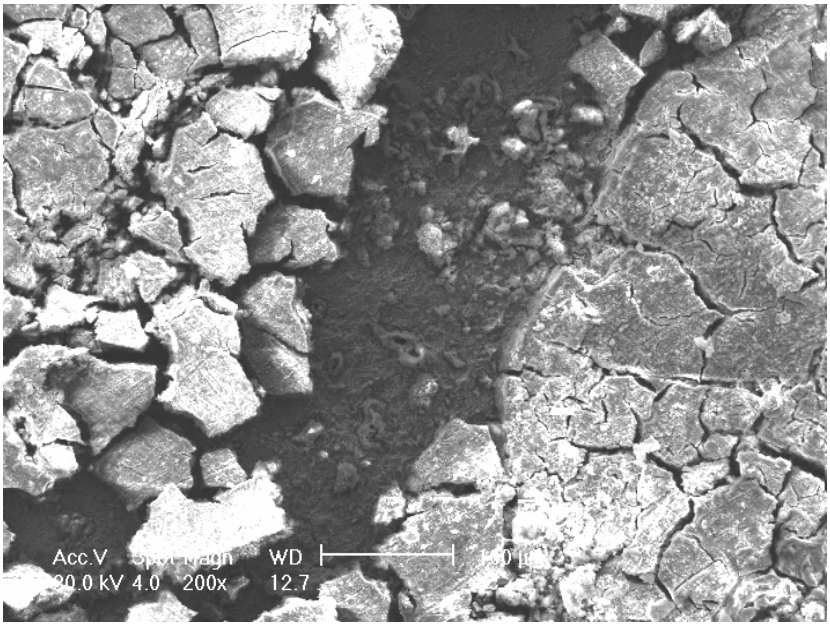

Figure 25. Experiment 3: Surface features of small UNS C1018 WL coupon from multiphase flow. SEM at 200X magnification shows multiple layers. (60°C, 0.77 MPa CO_2, pH 6, H_2S gas phase concentration = 120 ± 10 ppm, 25 day exposure).

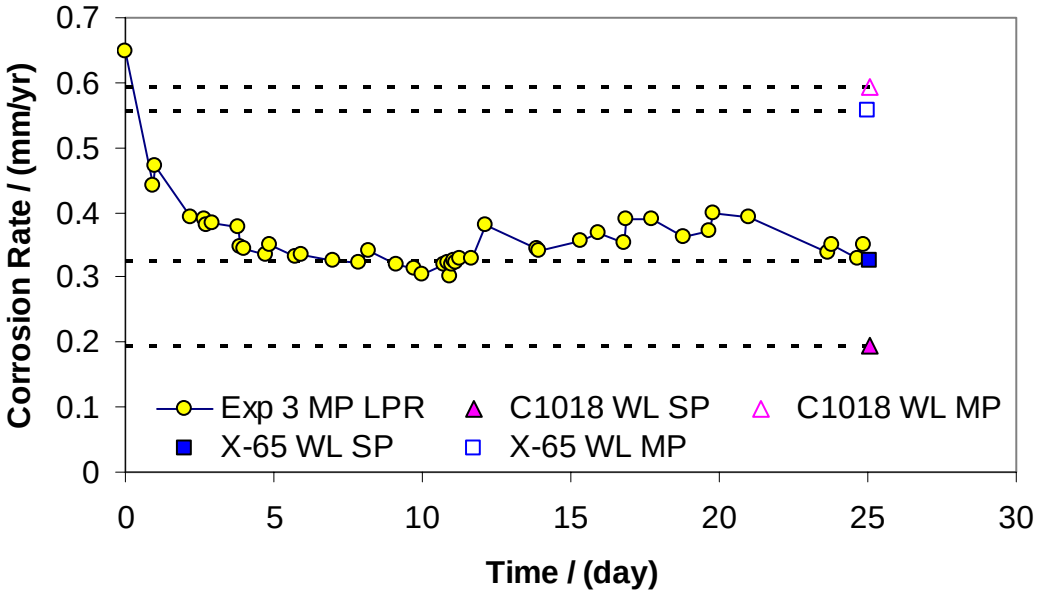

Figure 26. Experiment 3: Multiphase LPR and small WL coupon corrosion rate measurements. (60°C, 0.77 MPa CO_2, pH 6, H_2S gas phase concentration = 120 ± 10 ppm).

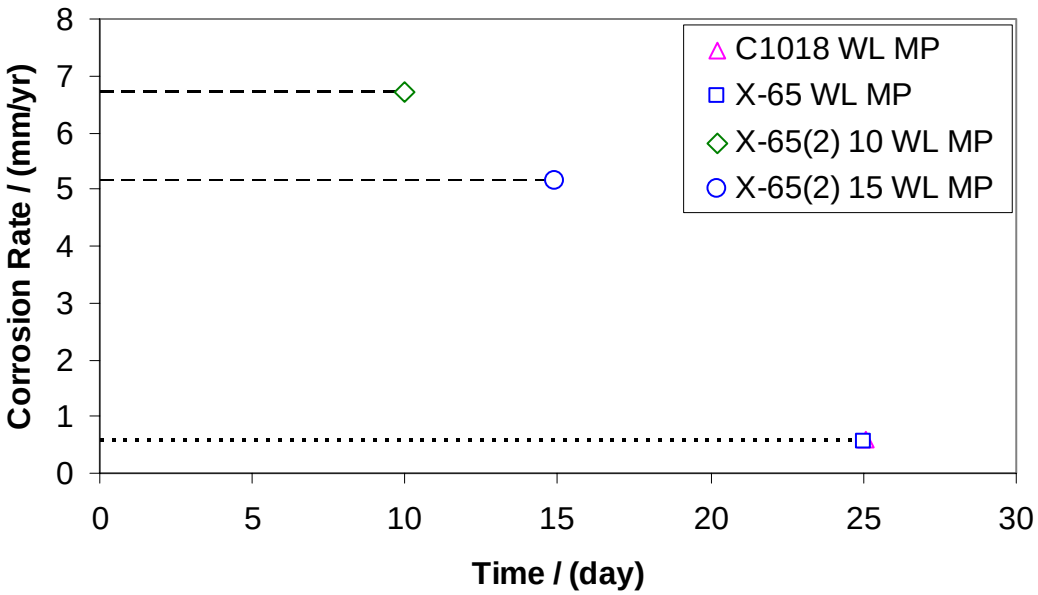

Figure 27. Experiment 3: Multiphase WL coupons. (60°C, 0.77 MPa CO_2, pH 6, H_2S gas phase concentration = 120 ± 10 ppm).

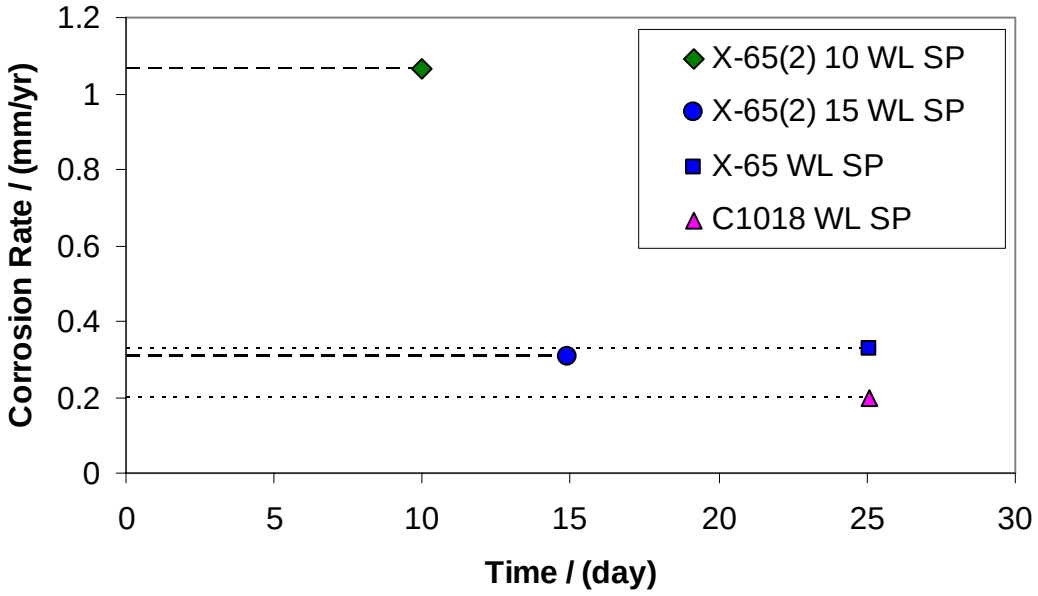

Figure 28. Experiment 3: Single phase WL coupons. (60°C, 0.77 MPa CO_2, pH 6, H_2S gas phase concentration = 120 ± 10 ppm)

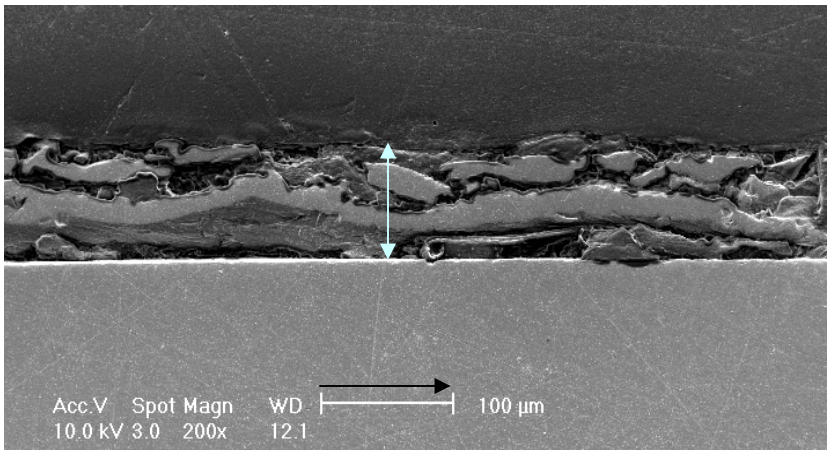

Figure 29. Experiment 3: Single phase UNS C1018 WL coupon cross section with 90µm total film thickness. SEM at 200X magnification shows multiple layers. (60°C, 0.77 MPa CO_2, pH 6, H_2S gas phase concentration = 120 ± 10 ppm, 25 day exposure).

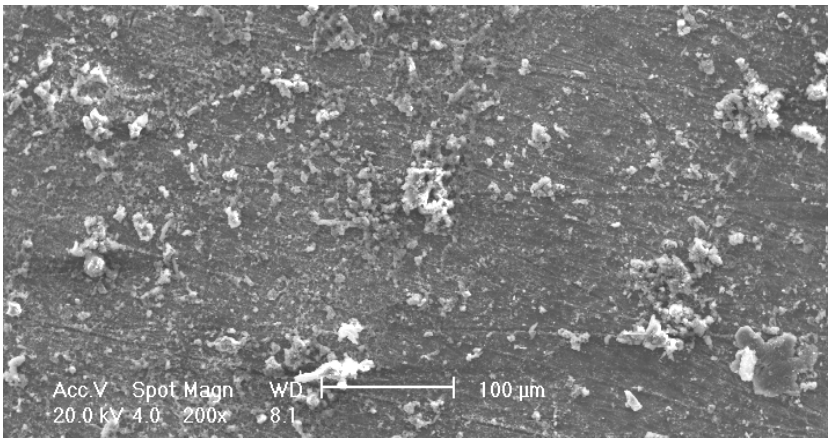

Figure 30. Experiment3: Single phase UNS C1018 WL coupon surface SEM at 200X. Uniform surface film coverage. (60°C, 0.77 MPa CO_2, pH 6, H_2S gas phase concentration = 120 ± 10 ppm, 25 day exposure).

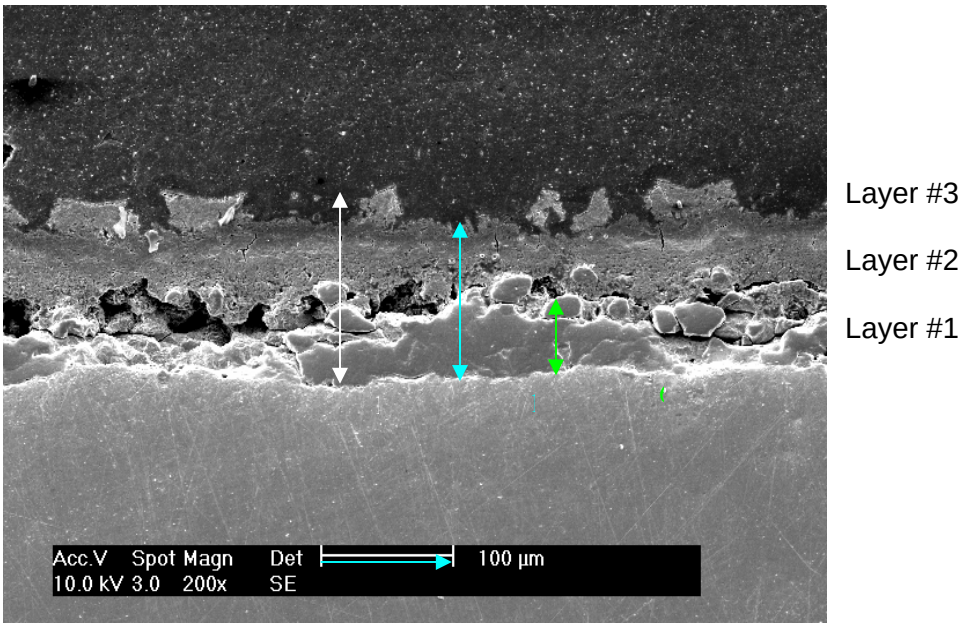

Figure 31. Experiment 3: Cross section of multiphase WL coupon after 25 day exposure. (60°C, 0.77 MPa CO_2, pH 6, H_2S gas phase concentration = 120 ± 10 ppm, 25 day exposure). Multiple layer film composition by EDS: layer #1 (next to metal surface, 60 µm) is [32.4% Fe, 0.0% S, 13.4% C, 26.5% O], the interface between layer #1 and layer #2 (60 µm) is [35.4% Fe, 12.9% S, 14.0% C, 9.5% O], and both layer #2 and layer #3 (30 µm) is [31.2% Fe, 15.0% S, 20.8% C, 11.2% O].

a)  b)  c) 

Figure 32. Experiment 1: X65(2) coupons exposed for (a) 10, (b) 20, and (c) 30 days. (60°C, 0.77 MPa CO_2, pH 6, 25 ± 10ppm H_2S).

a)  b)  c) 

Figure 33. Experiment 2: X65(2) coupons exposed for (a) 10, (b) 20, and (c) 30 days. (60°C, 0.77 MPa CO_2, pH 6, 12 ± 5ppm H_2S).

a)  b)  c) 

Figure 34. Experiment 3: X65(2) coupons exposed for (a) 10, (b) 15, and (c) 25 days. (60°C, 0.77 MPa CO_2, pH 6, 12 ± 5ppm H_2S).

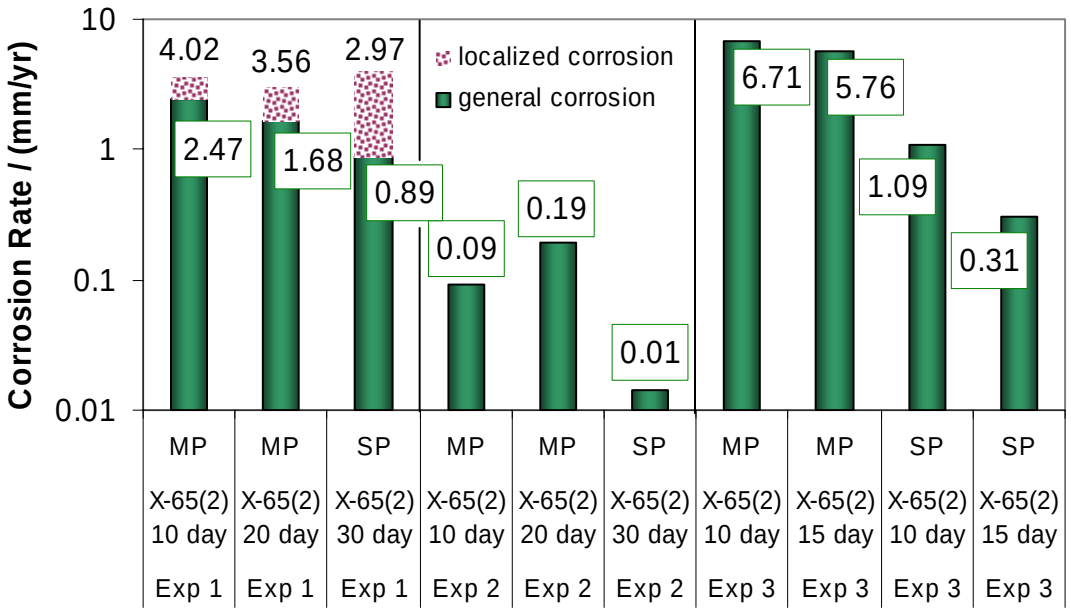

Figure 35. Large X65(2) coupon comparison from Experiment 1, 2, and 3. All corrosion rate values shown are in mm/yr. SP = single phase, MP = multiphase. (10, 20, and 30 day exposures)

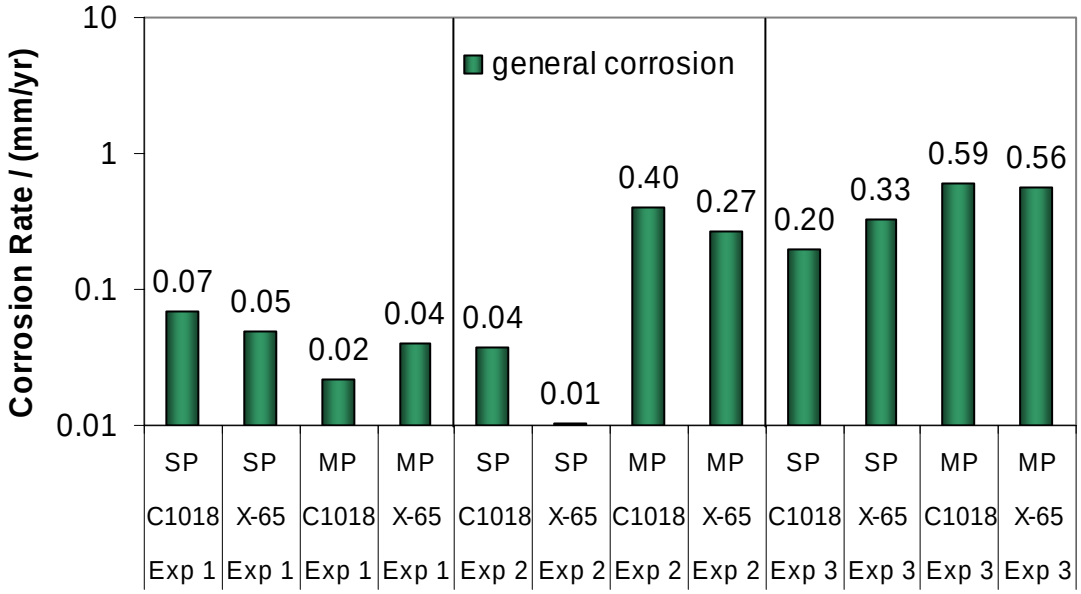

Figure 36. Small coupon comparison from Experiment 1, 2, and 3 by corrosion rate. All corrosion rate values shown are in mm/yr. SP = single phase, MP = multiphase. (60°C, 0.77 MPa CO_2, pH 6, 30 day exposures)